The Practical Behavior of Various Edge-Diffraction Formulas

Gregory D. Durgin

Georgia Institute of Technology
777 Atlantic Ave., Atlanta, GA 30332-0250 USA
Tel: +1 (404) 894-2951; Fax: +1 (404) 894-5935; E-mail: durgin@gatech.edu

Abstract

The scalar knife-edge diffraction (KED) solution is a workhorse for RF and optics engineers who regularly encounter practical diffraction phenomena. However, the approximate, polarization-independent KED result is formulated in a way that does not provide direct physical insight. In this article, we demonstrate how the KED formula contains similar underlying physics to other more-rigorous half-screen diffraction solutions, allowing engineers to apply common Geometrical Theory of Diffraction (GTD) formulations for *all* screen diffraction problems. The underlying geometrical behavior of the scalar KED solution sheds new light on these old problems, revealing why it is so useful for solving real-word problems in radiowave propagation.

Keywords: Diffraction; electromagnetic diffraction; geometrical theory of diffraction; acoustic diffraction; terrain factors; radio propagation; wedges

1. Introduction

This article presents a uniquely congruent development of both the knife-edge diffraction (KED) and Sommerfeld half-plane diffraction formulas. This development should help engineers understand when and how to apply these solutions. Despite their similarity and utility in quantifying diffraction phenomena, the Sommerfeld and KED solutions are rarely mentioned in the same breath, due to their vastly different formulations. To this point, Sommerfeld's solution is an exact result that requires solving a set of integral equations under plane-wave incidence [1]. On the other hand, the KED solution results from an approximate evaluation of the Kirchhoff-Helmholtz integral theorem, which itself is evaluated for the approximate Kirchhoff boundary conditions of a blocking screen. However, the analysis in this paper clearly shows the inter-relationship between the two solutions.

We build on the observations of Giovaneli in [2] to provide the diffraction pattern of the KED result, and to extend its existing usefulness [3]. Formulated from scalar diffraction theory, the KED result is polarization-independent, but can handle point-source radiators. Unlike the Sommerfeld result, it is surprisingly difficult to achieve a skewed angle-of-incidence KED solution. Multiple diffractions are also difficult to construct from KED, with numerous attempts that rely on correction factors and virtual sources reported in the research literature [4-7]. However, KED is particularly powerful in one sense: its direct extrapolation of incident fields without relying on integral equations allows the KED approach to be used in the analysis of perturbations of the knife-edge solution. For example, Davis and Brown have used it to study the effects of random edge roughness on the half-screen-diffracted-field solution [8].

The parallel analysis of these classical results sheds some new light on old problems. Key results are Figures 3-5, which illustrate amplitude and phase behaviors of the solutions. The most profound result is Figure 7, which shows that the diffracted portion of the KED solution is *precisely* the geometric mean of the Sommerfeld diffracted waves for parallel and perpendicular polarizations at normal incidence [9]. By demonstrating common underlying geometries in the Sommerfeld and KED results, we arrive at the common *Geometrical Theory of Diffraction* (GTD) formulation that achieves benefits of both. We conclude with an example of double terrain diffraction, which serves to illustrate the differences and tradeoffs between diffraction solutions. The ensuing physical understanding will help engineers choose which scenarios are more applicable to KED or Sommerfeld screen solutions.

2. Breaking Down Edge-Diffraction Formulas

2.1 Knife-Edge Diffraction Formula

The KED problem is formulated for a semi-infinite half-plane in between a point source and an observation point, as shown in Figure 1. A line drawn from the source to the observation point will thus clear the diffracting knife edge by a distance d. A negative value of d implies obstruction. The solution for this case is the famous KED formula [1]:

 ISSN 1045-9243/2009/$25 ©2009 IEEE

$$E_{\Diamond} = \left(\frac{1+j}{2}\right)\frac{E_0 \exp\left[-jk\left(r_0+r\right)\right]}{k\left(r+r_0\right)}\sqrt{\frac{2}{\pi}}\mathrm{F}\left[-d\sin\phi_i\sqrt{\frac{k}{2}\left(\frac{1}{r_0}+\frac{1}{r}\right)}\right], \tag{1}$$

where k is the wavenumber ($k = 2\pi/\lambda$) and r, r_0, d, and θ are geometrical terms summarized in Figure 1. $\mathrm{F}(\bullet)$ is the Fresnel integral function:

$$\mathrm{F}(a) = \int_a^{\infty} \exp\left(-j\tau^2\right) d\tau . \tag{2}$$

The KED result presumes an isotropic radiator of the form

$$E_{\Diamond i} = \frac{E_0 \exp\left[-jk\left(r_0+r\right)\right]}{k\left(r_0+r\right)} \tag{3}$$

on the source side of the screen. Equation (1) is an approximate result, independent of incident-field polarization (the $\Diamond$ subscript is used in this work to denote a scalar result). However, it has proven to be resilient and useful for both optics and radiowave propagation.

There is a powerful geometrical interpretation of Equation (1) that allows it to be recast in terms of distances between the line-of-sight (LOS) path, $r+r_0$, and the total length of the two line segments formed from source-to-edge-to-observation. This difference may be expressed mathematically as Δr:

$$\begin{aligned}\Delta r &= \overbrace{\sqrt{r_0^2+d'^2}}^{\text{source-to-edge}} + \overbrace{\sqrt{r^2+d'^2}}^{\text{edge-to-observation}} - \overbrace{\left(r+r_0\right)}^{\text{LOS path}} \\ &\approx r_0\left(1+\frac{d'^2}{2r_0^2}\right)+r\left(1+\frac{d'^2}{2r^2}\right)-\left(r+r_0\right) \\ &\approx \frac{d'^2}{2}\left(\frac{1}{r_0}+\frac{1}{r}\right).\end{aligned} \tag{4}$$

Interestingly, the square root of this term (multiplied by k) is precisely the argument of the Fresnel integral function that describes the principle amplitude changes in Equation (1). For a fixed difference in path length, Δr, there are two sets of solutions for modified clearance distance, d', which will maintain a constant Fresnel integral function argument:

$$d' = \pm\sqrt{\frac{2r_0 r\Delta r}{r+r_0}} . \tag{5}$$

Collecting either the positive or negative roots in Equation (5) produces a set of d' values as a function of r and r_0 that results in constant-amplitude electric field at the receiver location. Furthermore, based on the geometrical definition in Figure 1, we can see that the set of all d' values satisfying Equation (5) for a given source-observation approximates an ellipse, the foci of which are the source and observation points.

Although ideal semi-infinite diffracting screens are hard to find in reality, radio engineers commonly use the KED result to approximate the effects of partial blockages in wireless links. Office buildings, trees, houses, terrain, and many other things have all been modeled as screens for the purposes of UHF and microwave radio diffraction [10-12]. In KED, the shape and orientation of the screen have only a secondary effect on the solution, anyway. Just consider Figure 1, where the screen can be oriented at nearly any angle and still produce nearly the same field solution in Equation (1), provided the edge produces the same clearance distance at d' for a given r and r_0.

In designing point-to-point microwave links, diffraction effects are minimized by ensuring enough clearance distance between the link line-of-sight path and the nearest diffracting element. To facilitate link design, ellipsoids of constant path difference are drawn around the link, with one focus at the transmitter and one focus at the receiver. This geometry is illustrated in Figure 2. The ellipsoids of interest occur for path differences

$$\text{Ellipsoid } n: \quad \Delta r = \frac{n\lambda}{2} \text{ for all points on ellipse.} \tag{6}$$

The regions between these constant ellipsoids are *Fresnel zones*, with the nth Fresnel zone defined as the region between the $(n-1)$th and nth ellipsoids of half-wavelength path difference. The nth Fresnel zone thus corresponds to clearance distances in the following range:

$$\sqrt{\frac{r_0 r\left(n-1\right)\lambda}{r+r_0}} < \left(d'\right)_n < \sqrt{\frac{r_0 rn\lambda}{r+r_0}} . \tag{7}$$

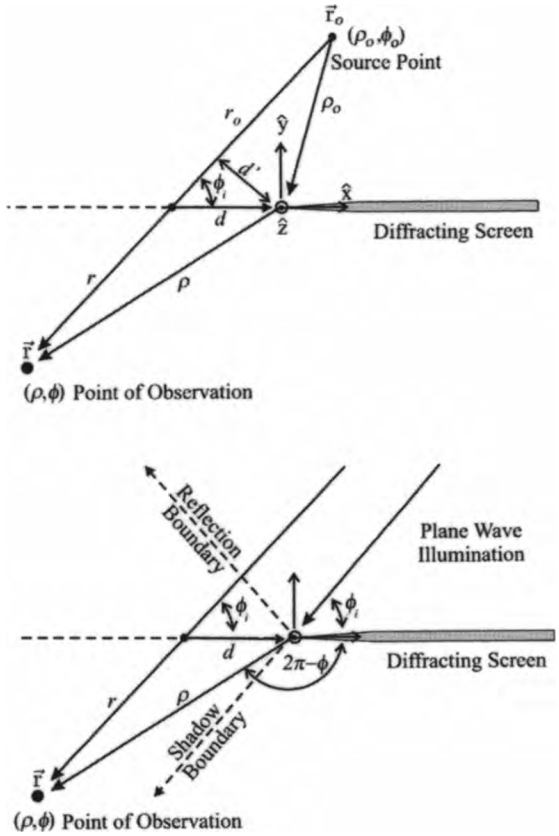

Figure 1. The geometry used for diffraction by a thin semi-infinite plane (i.e., a "knife edge").

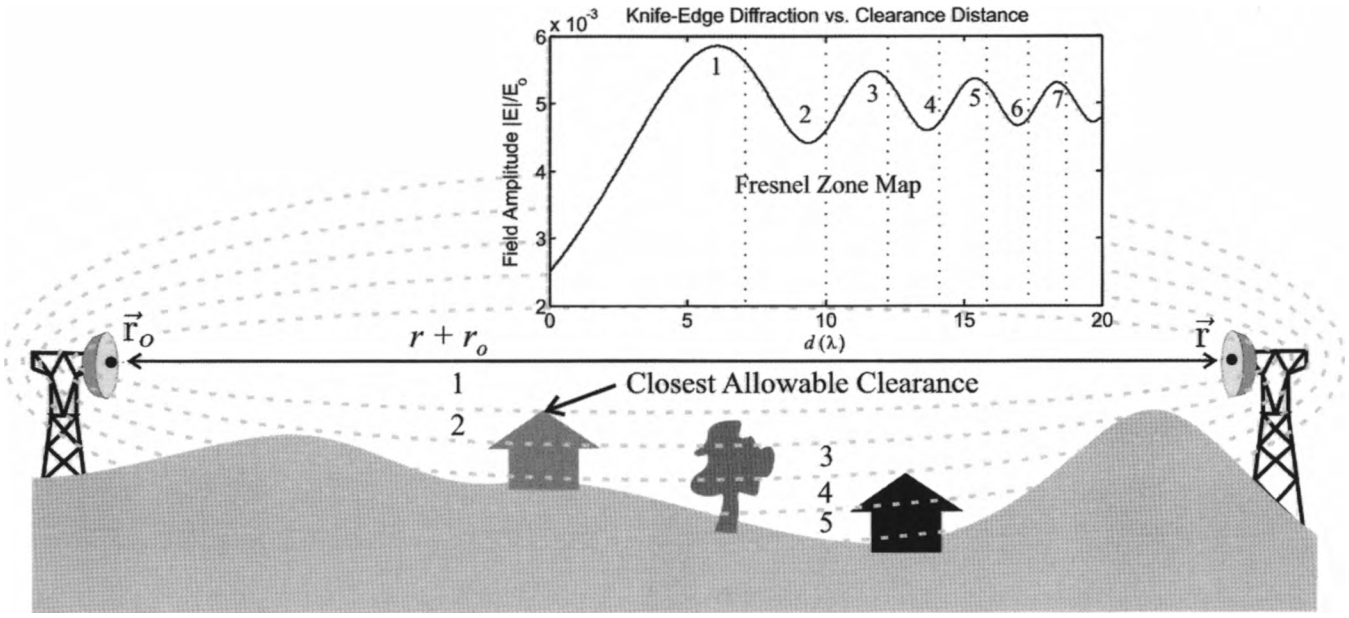

Figure 2. The geometry of Fresnel-zone ellipsoids clearing obstacles in a microwave link. The Fresnel zones are labeled moving from the first ellipsoid outward.

The practical significance of the Fresnel zones can be shown by magnifying the KED solution in Figure 2 for regions of small clearance. Generally, odd zones are regions of constructive interference, and even zones are regions of destructive interference.

2.2 Sommerfeld Solution for the PEC Edge

The exact Sommerfeld solution of the PEC half-plane problem depends on the polarization of the incident field. In this discussion, *perpendicular* ($\perp$) polarization refers to an incident plane wave with electric field perpendicular to the plane of incidence (the sheet of paper in Figure 1): the electric-field vector will have only a z component. In diffraction literature, this case is often called *soft polarization* – an artifact of acoustic propagation theory. *Parallel* ($\parallel$) polarization refers to an incident plane wave with electric field parallel to the plane of incidence: the electric-field vector will have only x and y components. This case is often called *hard polarization*.

Marking three regions of space in Figure 1 helps the discussion of the Sommerfeld solution. The *reflection region* is the area defined by $0 \le \phi < 180° - \phi_i$. In this region, Geometrical Optics predicts the total field to be the superposition of two uniform plane waves: the incident and reflected waves. The *incident region* is the area defined by $180° - \phi_i \le \phi \le 180° + \phi_i$. In this region, Geometrical Optics would predict the total field to be only the incident plane wave. Finally, the *shadow region* is the area defined by $180° + \phi_i < \phi < 360°$. Geometrical Optics predicts the total field to be zero in this region, as the incident wave has been shielded entirely by the PEC. The exact total-field solution for both types of polarization, along with the mathematical forms of the incident waves, are summarized in Table 1 using the cylindrical-coordinate geometry in Figure 1 [1].

The Sommerfeld solution is a convenient construction, but does not provide immediate intuition or insight into the wave propagation. To remedy this, let us use the following formulation for total electric field $\vec{E}$:

$$\vec{E} = \vec{E}_{GO} + \vec{E}_d , \tag{8}$$

where $\vec{E}_{GO}$ is the Geometrical Optics solution in Table 1, and $\vec{E}_d$ is the *diffracted field* solution. The amplitudes and phases of the total $\vec{E}$, Geometrical Optics $\vec{E}_{GO}$, and diffracted $\vec{E}_z$ fields for perpendicular incidence are illustrated in Figure 3, demonstrating how the discontinuities in the diffracted field exactly counterbalance the discontinuities in the Geometrical Optics field. Note the interesting phase behavior in the diffracted field: the phase tapers linearly in a circular pattern away from the screen's edge. Of course, the same behavior is present in the diffracted H_z fields for parallel incidence, which is shown in Figure 4. The results confirm Keller's initial GTD assumption that wave-diffraction effects are approximately localized to material discontinuities [13].

2.3 Comparing KED with the Sommerfeld Solution

It is a useful exercise to transform the KED solution into the same geometry as the Sommerfeld half-plane problem, and to perform the same Geometrical Optics plus diffracted wave decomposition of fields as in Equation (8). Keeping in mind that the KED solution is valid only on one side of the diffracting screen, Figure 5 illustrates the amplitudes and phases of the total, Geometrical Optics, and diffracted fields of KED. Two immediate behaviors become evident: 1) KED diffraction exhibits a localized wave that emanates from the edge and superimposes onto the total Geometrical Optics field; and 2) due to the KED approximations, there is a "fish-eye" distortion in the phase of this localized wave that becomes severe at angles of observation approaching $\phi \to 180°$ and $\phi \to 360°$. However, the amplitude of the localized wave still satisfies the Kirchhoff boundary conditions by approaching zero on the plane of the half-screen.

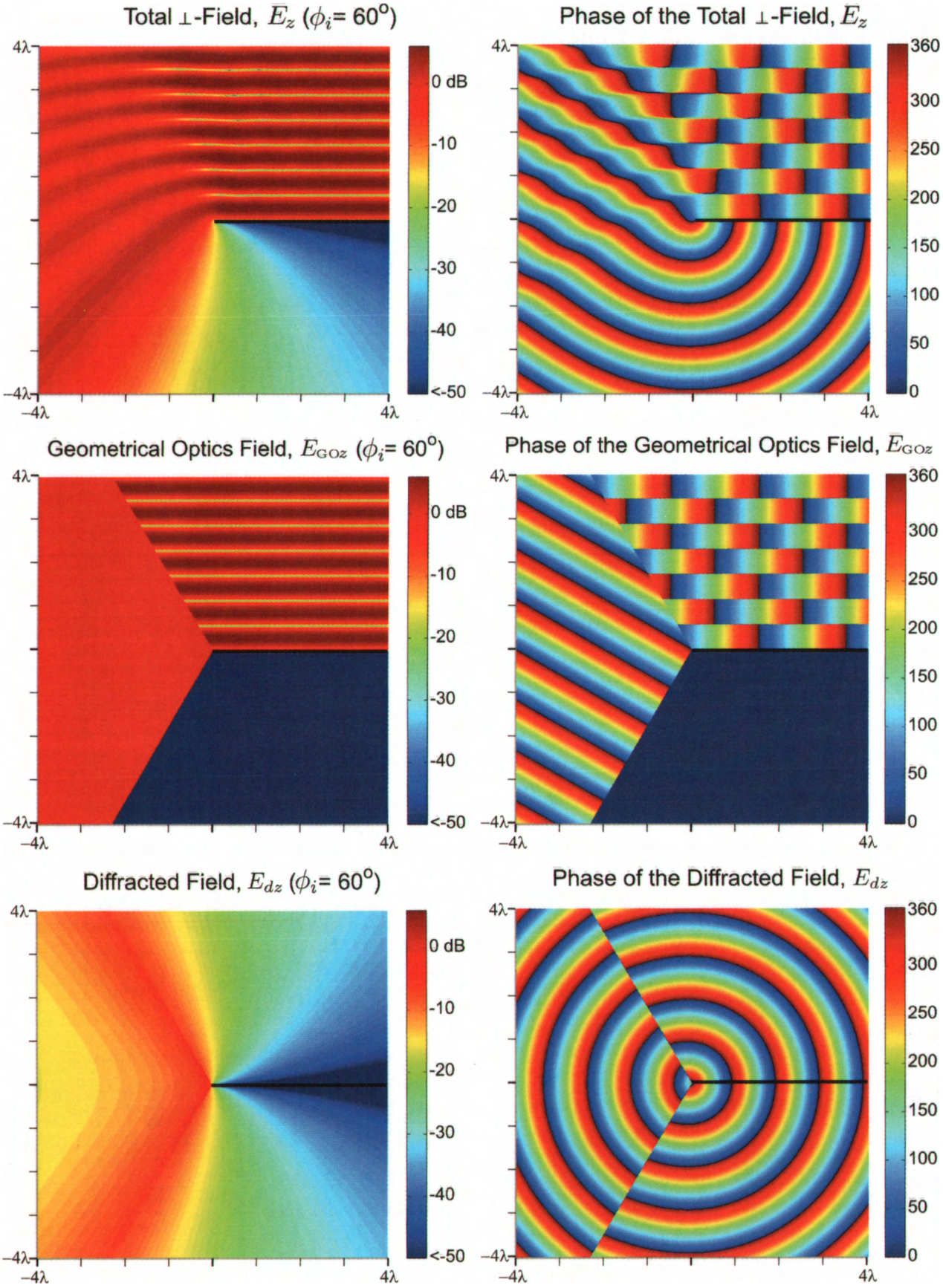

Figure 3. The amplitude and phase of the ⊥-incident Sommerfeld solution for an incident plane wave at $\phi_i = 60°$. All amplitudes were graphed in dB with respect to the magnitude of the incident plane wave.

3. GTD Interpretation

3.1 Sommerfeld Asymptotic Expansion

We will concentrate on perpendicular incidence for our asymptotic analysis, as the parallel incidence similarly follows. First, note that the diffracted field in this formulation may be written as

$$E_{dz} = \frac{E_0 \exp\left(\frac{j\pi}{4}\right)}{\sqrt{\pi}} \left\{ \mp \exp\left[jk\rho\cos\left(\phi - \phi_i\right)\right] \mathrm{F}\left[\pm\sqrt{2k\rho}\cos\left(\frac{\phi-\phi_i}{2}\right)\right] \right.$$
$$\left. \pm \exp\left[jk\rho\cos\left(\phi + \phi_i\right)\right] \mathrm{F}\left[\pm\sqrt{2k\rho}\cos\left(\frac{\phi+\phi_i}{2}\right)\right] \right\}, \qquad (9)$$

Top sign: Reflection Region, $\phi \le \pi - \phi_i$

Middle sign: Incidence Region, $\pi - \phi_i < \phi \le \pi + \phi_i$

Bottom sign: Shadow Region, $\phi > \pi + \phi_i$

where the three signs mark the three discontinuous regions that exist in the Geometrical Optics solution that persist when subtracted from the Sommerfeld solution in Table 1. Equation (9) makes use of the identity

$$\mathrm{F}(a) = \sqrt{\pi}\exp\left(-\frac{j\pi}{4}\right) - \mathrm{F}(-a), \qquad (10)$$

which cancels subtracted plane-wave terms so that the solution may always be expressed in terms of Fresnel integral functions.

Half-plane formulations are convenient in asymptotic analysis, since a working expansion can be achieved simply by integrating the Fresnel integral function repeatedly by parts:

$$\mathrm{F}(a) = \underbrace{-\frac{j}{2a}\exp\left(-ja^2\right)}_{O(1/a)} + \underbrace{\frac{1}{4a^3}\exp\left(-ja^2\right)}_{O(1/a^3)} - \underbrace{\frac{1}{12}\int_a^\infty \frac{1}{x^4}\exp\left(-jx^2\right)dx}_{O(1/a^5)\ +\ \text{higher-order terms}} \qquad (11)$$

Table 1. A summary of the Sommerfeld half-plane diffraction solutions.

Total Field Solution for ⊥ Polarization

$$E_z = \frac{E_0 \exp\left(\frac{j\pi}{4}\right)}{\sqrt{\pi}} \left\{ \exp\left[jk\rho\cos\left(\phi - \phi_i\right)\right] \mathrm{F}\left[-\sqrt{2k\rho}\cos\left(\frac{\phi-\phi_i}{2}\right)\right] - \exp\left[jk\rho\cos\left(\phi + \phi_i\right)\right] \mathrm{F}\left[-\sqrt{2k\rho}\cos\left(\frac{\phi+\phi_i}{2}\right)\right] \right\}$$

$$H_\rho = \frac{E_0 \exp\left[j\left(\frac{\pi}{4} - k\rho\right)\right]}{\eta\sqrt{\pi}} \left\{ \sin\left(\phi - \phi_i\right) \mathrm{G}\left[-\sqrt{2k\rho}\cos\left(\frac{\phi-\phi_i}{2}\right)\right] - \sin\left(\phi + \phi_i\right) \mathrm{G}\left[-\sqrt{2k\rho}\cos\left(\frac{\phi+\phi_i}{2}\right)\right] + j\sqrt{\frac{2}{k\rho}}\sin\frac{\phi_i}{2}\cos\frac{\phi}{2} \right\}$$

$$H_\phi = \frac{E_0 \exp\left[j\left(\frac{\pi}{4} - k\rho\right)\right]}{\eta\sqrt{\pi}} \left\{ \cos\left(\phi - \phi_i\right) \mathrm{G}\left[-\sqrt{2k\rho}\cos\left(\frac{\phi-\phi_i}{2}\right)\right] - \cos\left(\phi + \phi_i\right) \mathrm{G}\left[-\sqrt{2k\rho}\cos\left(\frac{\phi+\phi_i}{2}\right)\right] - j\sqrt{\frac{2}{k\rho}}\sin\frac{\phi_i}{2}\sin\frac{\phi}{2} \right\}$$

Incident Wave: $E_z = E_0 \exp\left[jk\rho\cos\left(\phi - \phi_i\right)\right]$; GO Reflection: $E_z = -E_0 \exp\left[jk\rho\cos\left(\phi + \phi_i\right)\right]$

Total Field Solution for ∥ Polarization

$$H_z = \frac{E_0 \exp\left(\frac{j\pi}{4}\right)}{\eta\sqrt{\pi}} \left\{ \exp\left[jk\rho\cos\left(\phi - \phi_i\right)\right] \mathrm{F}\left[-\sqrt{2k\rho}\cos\left(\frac{\phi-\phi_i}{2}\right)\right] + \exp\left[jk\rho\cos\left(\phi + \phi_i\right)\right] \mathrm{F}\left[-\sqrt{2k\rho}\cos\left(\frac{\phi+\phi_i}{2}\right)\right] \right\}$$

$$E_\rho = \frac{E_0 \exp\left[j\left(\frac{\pi}{4} - k\rho\right)\right]}{\sqrt{\pi}} \left\{ -\sin\left(\phi - \phi_i\right) \mathrm{G}\left[-\sqrt{2k\rho}\cos\left(\frac{\phi-\phi_i}{2}\right)\right] - \sin\left(\phi + \phi_i\right) \mathrm{G}\left[-\sqrt{2k\rho}\cos\left(\frac{\phi+\phi_i}{2}\right)\right] + j\sqrt{\frac{2}{k\rho}}\sin\frac{\phi_i}{2}\cos\frac{\phi}{2} \right\}$$

$$E_\phi = \frac{E_0 \exp\left[j\left(\frac{\pi}{4} - k\rho\right)\right]}{\sqrt{\pi}} \left\{ -\cos\left(\phi - \phi_i\right) \mathrm{G}\left[-\sqrt{2k\rho}\cos\left(\frac{\phi-\phi_i}{2}\right)\right] - \cos\left(\phi + \phi_i\right) \mathrm{G}\left[-\sqrt{2k\rho}\cos\left(\frac{\phi+\phi_i}{2}\right)\right] - j\sqrt{\frac{2}{k\rho}}\cos\frac{\phi_i}{2}\cos\frac{\phi}{2} \right\}$$

Incident Wave: $H_z = \frac{E_0}{\eta}\exp\left[jk\rho\cos\left(\phi - \phi_i\right)\right]$; GO Reflection: $H_z = \frac{E_0}{\eta}\exp\left[jk\rho\cos\left(\phi + \phi_i\right)\right]$

Fresnel Integral Function: $\mathrm{F}(a) = \int_a^\infty \exp\left(-j\tau^2\right)d\tau$; **Helper Function:** $\mathrm{G}(a) = \exp\left(ja^2\right)\mathrm{F}(a)$

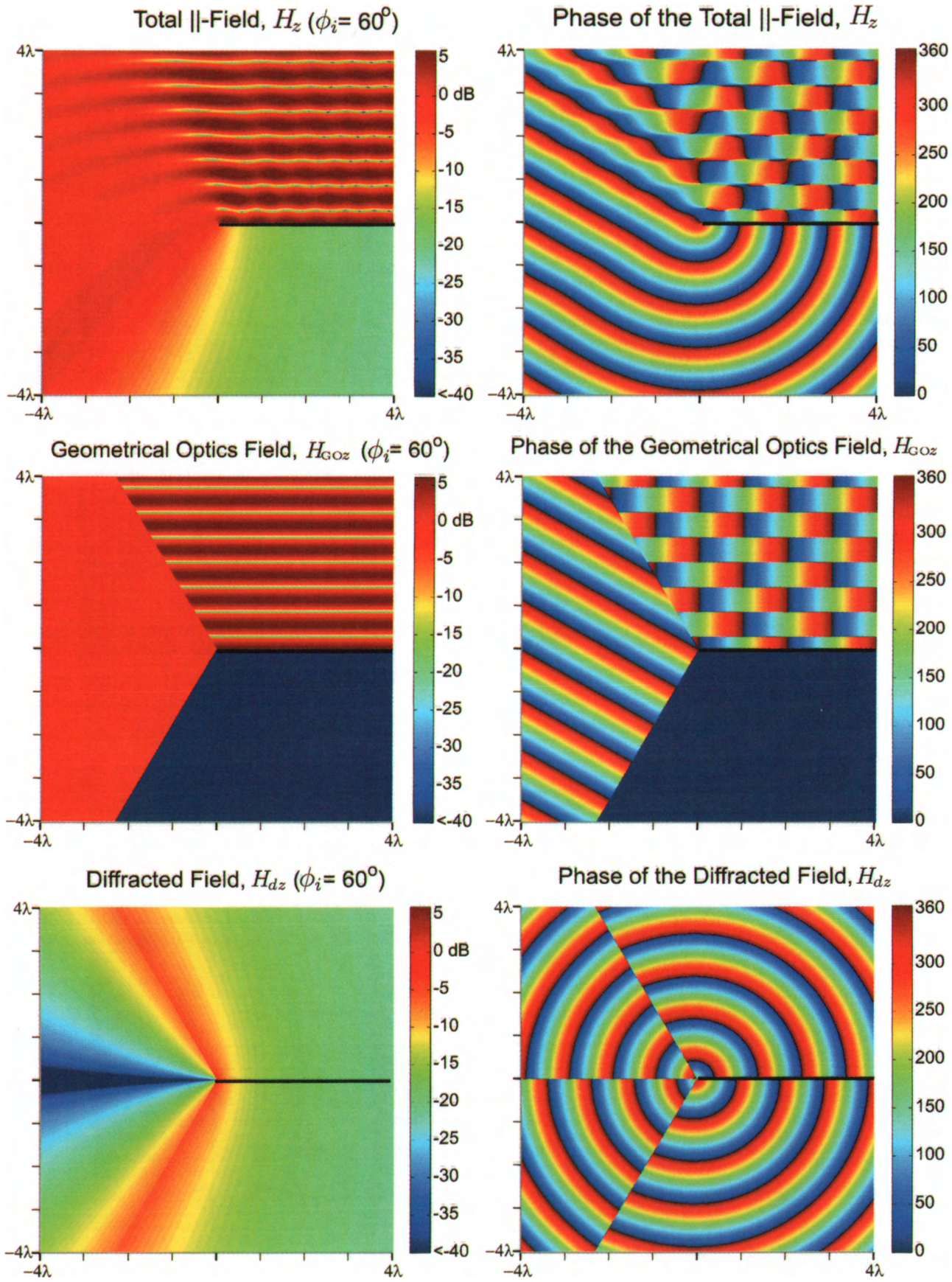

Figure 4. The amplitude and phase of the ‖-incident Sommerfeld solution for an incident plane wave at $\phi_i = 60°$. All amplitudes were graphed in dB with respect to the magnitude of the incident plane wave.

This method does not get any closer to a closed-form result for the integral, but we have generated a series expansion with respect to $1/a$. Keeping only the first term in Equation (11) and ignoring the higher-order behavior, the diffracted field of Equation (9) may be written as

$$E_{dz}(\rho,\phi) \approx E_0 \overbrace{\frac{\exp(-jk\rho)}{\sqrt{k\rho}}}^{\text{cylindrical wave}} \overbrace{\frac{-\exp\left(-\frac{j\pi}{4}\right)}{2\sqrt{2\pi}}\left[\sec\left(\frac{\phi-\phi_i}{2}\right)-\sec\left(\frac{\phi+\phi_i}{2}\right)\right]}^{D_\perp(\phi,\phi_i)\text{ diffraction pattern}} \tag{12}$$

which should be valid for arguments of the Fresnel integral function corresponding to $a>1$ [14]. The approximate diffracted field has now taken on the form of a cylindrical wave emanating from the diffracting edge. Furthermore, there is a ϕ-varying pattern to this wave that matches the Keller GTD screen-diffraction coefficient [13].

The diffraction pattern in Equation (12) is an accurate approximation when the cylindrical edge wave superimposes atop the Geometrical Optics wave, both of which are easy to construct. The approximation only fails close in to either the shadow or reflection boundary, where the argument of the approximated Fresnel integral functions becomes small. In fact, this condition – where the Fresnel argument $a \le 1$ – defines a pair of parabolic regions around the shadow and reflection boundaries. As the observation point moves farther from the diffracting edge, the region about these boundaries where Equation (12) is invalid becomes smaller *relative* to the distance from the edge. The *Uniform Theory of Diffraction* correction to GTD, as originally formulated by Kouyoumjian and Pathak, can be used to improve the solution within these parabolic regions [15].

Note that a diffraction coefficient for parallel polarization follows similarly; both coefficients are summarized in Table 2.

3.2 KED Asymptotic Expansion

Proceeding in a similar fashion, we may subtract out the Geometrical Optics portion of the KED solution from Equation (1) over the region $\phi < \phi_i + \pi$ to achieve the diffracted field:

$$E_d = \mp\sqrt{\frac{2}{\pi}}\left(\frac{1+j}{2}\right)\frac{E_0\exp[-jk(r_0+r)]}{k(r+r_0)}\mathrm{F}\left[\pm d\sin\phi_i\sqrt{\frac{k}{2}\left(\frac{1}{r_0}+\frac{1}{r}\right)}\right], \tag{13}$$

where the top signs are valid for the incidence region ($\phi < \phi_i + \pi$) and the bottom signs are valid for the shadowed region ($\phi > \phi_i + \pi$). Based on the geometry of the problem, we may recast this in terms of the path-length difference Δr, defined in Equation (4):

$$E_d(\rho,\phi) = \mp\sqrt{\frac{2}{\pi}}\left(\frac{1+j}{2}\right)\frac{E_0\exp\left[-jk(\rho_0+\rho-\Delta r)\right]}{k(\rho_0+\rho-\Delta r)}\mathrm{F}\left(\pm\sqrt{k\Delta r}\right) \tag{14}$$

Using the same expansion for the Fresnel integral function as in Equation (10), we may write the approximate diffracted field as

$$E_d(\rho,\phi) \approx \left\{\underbrace{\frac{E_0}{k\rho_0}\exp(-jk\rho_0)}_{\text{incident field}}\underbrace{\frac{\exp(-jk\rho)}{\sqrt{k\rho}}\sqrt{\frac{\rho_0}{\rho_0+\rho}}}_{\text{diffracted wave}}\right\} \left\{\underbrace{\frac{-1}{2\sqrt{\pi}}\exp\left(-j\frac{\pi}{4}\right)\frac{\sqrt{\rho_0\rho(\rho_0+\rho)}}{(\rho_0+\rho-\Delta r)\sqrt{\Delta r}}}_{\text{diffraction coefficient}}\right\} \tag{15}$$

The diffraction coefficient (all of the leftover terms in the solution) should be relatively insensitive to the source distance ρ_0 from the edge, as GTD would predict. We may thus take the limit as $\rho_0 \to \infty$, which would correspond to plane-wave incidence:

$$D_\Diamond(\phi,\phi_i) = \frac{-1}{2\sqrt{\pi}}\exp\left(-j\frac{\pi}{4}\right)\sqrt{\frac{\rho}{\Delta r}}. \tag{16}$$

This coefficient resembles one obtained by Giovaneli in [2]. Based on the plane-wave geometry, the law of sines may be applied in Figure 1 to simplify the diffracted-wave solution [9]:

$$\sqrt{\frac{\rho}{\Delta r}} = \sqrt{\frac{2r\rho}{d^2\sin^2\phi_i}} = \frac{1}{\left|\sin(\phi-\phi_i)\right|}\sqrt{-\frac{2\sin\phi}{\sin\phi_i}}. \tag{17}$$

Table 2. A summary of the half-plane GTD diffraction coefficients.

Solution Type	Diffraction Coefficient
Sommerfeld-$\perp$	$D_\perp(\phi,\phi_i) = \frac{-\exp\left(-j\frac{\pi}{4}\right)}{2\sqrt{2\pi}}\left[\sec\left(\frac{\phi-\phi_i}{2}\right)-\sec\left(\frac{\phi+\phi_i}{2}\right)\right]$
Sommerfeld-$\parallel$	$D_\parallel(\phi,\phi_i) = \frac{-\exp\left(-j\frac{\pi}{4}\right)}{2\sqrt{2\pi}}\left[\sec\left(\frac{\phi-\phi_i}{2}\right)+\sec\left(\frac{\phi+\phi_i}{2}\right)\right]$
Felsen Absorber	$D_\Diamond^{(F)}(\phi,\phi_i) = \frac{-\exp\left(-j\frac{\pi}{4}\right)}{\sqrt{2\pi}}\left[\frac{1}{\pi-\lvert\phi-\phi_i\rvert}+\frac{1}{\pi+\lvert\phi-\phi_i\rvert}\right]$
KED Blockage	$D_\Diamond(\phi,\phi_i) = \frac{-\exp\left(-j\frac{\pi}{4}\right)}{\sqrt{2\pi}}\lvert\csc(\phi-\phi_i)\rvert\sqrt{-\frac{\sin\phi}{\sin\phi_i}}$

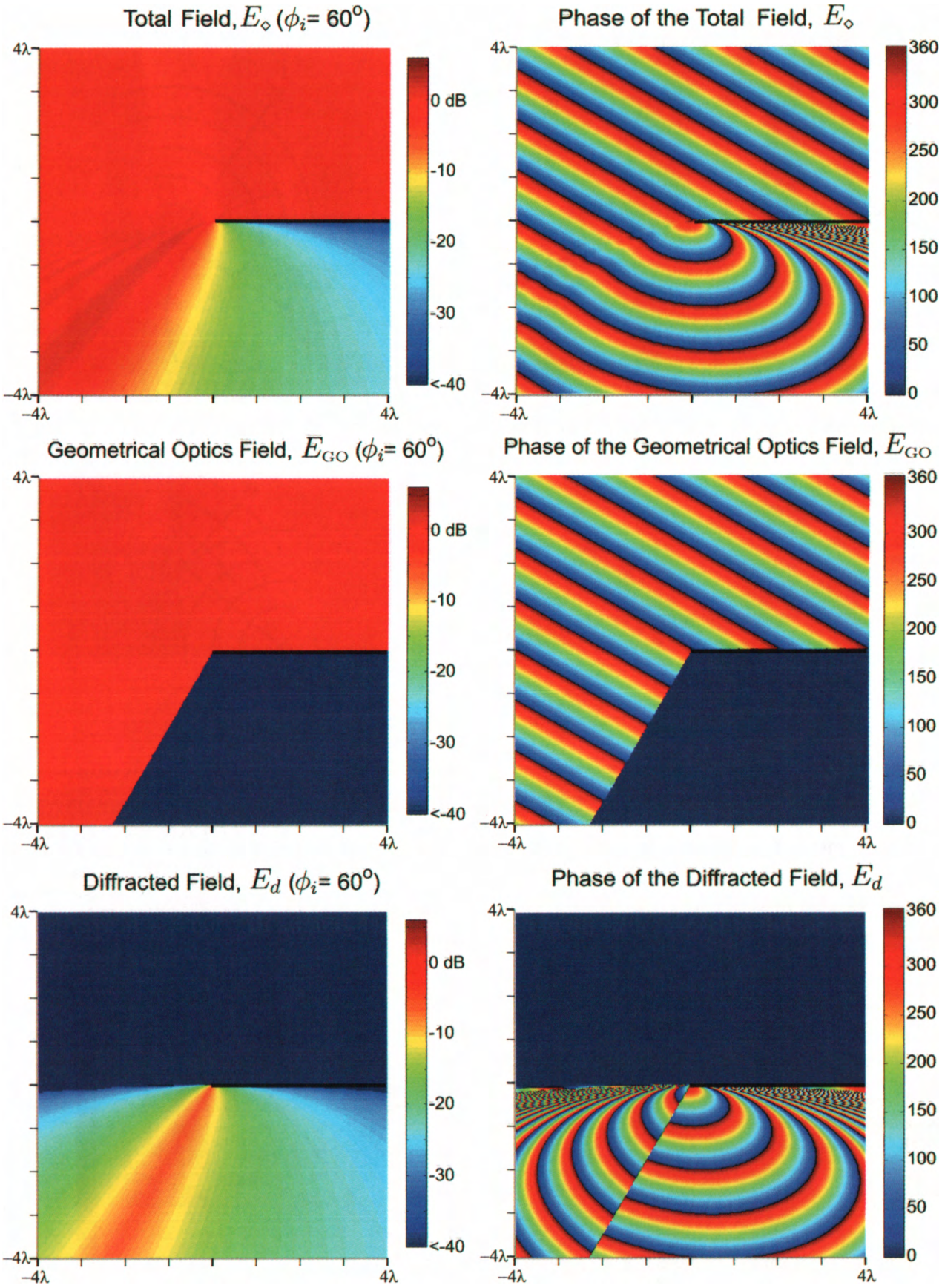

Figure 5. The amplitude and phase of the knife-edge diffraction solution for an incident plane wave at $\phi_i = 60°$. All amplitudes were graphed in dB with respect to the magnitude of the incident plane wave.

After substitutions and simplifications, the diffraction coefficient may be expressed solely as a function of angular geometry. The end result is summarized in Table 2. Using this method of derivation, the KED diffraction coefficient differs from an alternative, normal-incident coefficient derived by Bertoni [16]. Bertoni's coefficient more closely resembles Felsen's GTD solution for a perfect absorber [17].

3.3 Extended GTD Formulation

Normal-incidence diffraction coefficients may be extended to skewed incidence, although the polarization effects can be difficult to track. Below is a generic algorithm for calculating GTD ray power for a variety of edge-diffraction problems:

1. Define the incident wavefront in terms of Geometrical Optics, tracking principle radii of curvature along the parallel-incident and perpendicular-incident directions with respect to the diffracting edge ($\rho_\parallel$ and $\rho_\perp$, respectively):

$$\vec{\mathrm{E}}_i(\vec{\mathrm{r}}) = E_0 \hat{\mathrm{e}}_i \sqrt{\frac{\rho_\perp \rho_\parallel}{(s+\rho_\perp)(s+\rho_\parallel)}} \exp(-jks), \quad s = \left\|\vec{\mathrm{r}} - \vec{\mathrm{r}}_0\right\|.$$

   For illumination by realistic point sources, $\rho_\parallel = \rho_\perp$.

2. Locate the point on a diffracting edge $\vec{\mathrm{r}}_d$ that satisfies $\theta_d = \theta_i$ in Figure 6 (the angle of the diffracted ray equals the angle of the incident ray), and evaluate the incident field here, $\vec{\mathrm{E}}_i(\vec{\mathrm{r}}_d)$.

3. Calculate the unit-less *dyadic diffraction coefficient* for the diffracting element based on geometry and material properties.

4. Construct the diffracted-wave solution using geometrical principles:

$$\vec{\mathrm{E}}_d(\vec{\mathrm{r}}) = \frac{\vec{\mathrm{E}}_i(\vec{\mathrm{r}}_d) \bullet \mathbf{D}(\phi, \phi_i)}{\sin\theta_d \sqrt{ks}} \sqrt{\frac{\rho_\perp}{\rho_\perp + s}} \exp(-jks), \quad s = \left\|\vec{\mathrm{r}} - \vec{\mathrm{r}}_d\right\|. \qquad (18)$$

   This is the wave that adds to the Geometrical Optics solution to provide an estimate of the diffracted field.

The key to this formulation is the dyadic diffraction coefficient, which takes the following form:

$$\mathbf{D}(\phi, \phi_i) = D_\perp(\phi, \phi_i)\hat{\mathrm{u}}_\perp\hat{\mathrm{v}}_\perp + D_\parallel(\phi, \phi_i)\hat{\mathrm{u}}_\parallel\hat{\mathrm{v}}_\parallel. \qquad (19)$$

The coefficient in Equation (19) is a *dyad* because of the pair of vectors that appears in the equation, representing an operation that converts a vector to another vector [18]. When applying the dot product of the incident-field vector to the dyadic diffraction coefficient, the product is taken with the leftward unit vectors, and the result is applied as a coefficient to the rightward unit vectors. Equation (19) collapses to a single scalar value when KED or similarly acoustic diffraction is applied.

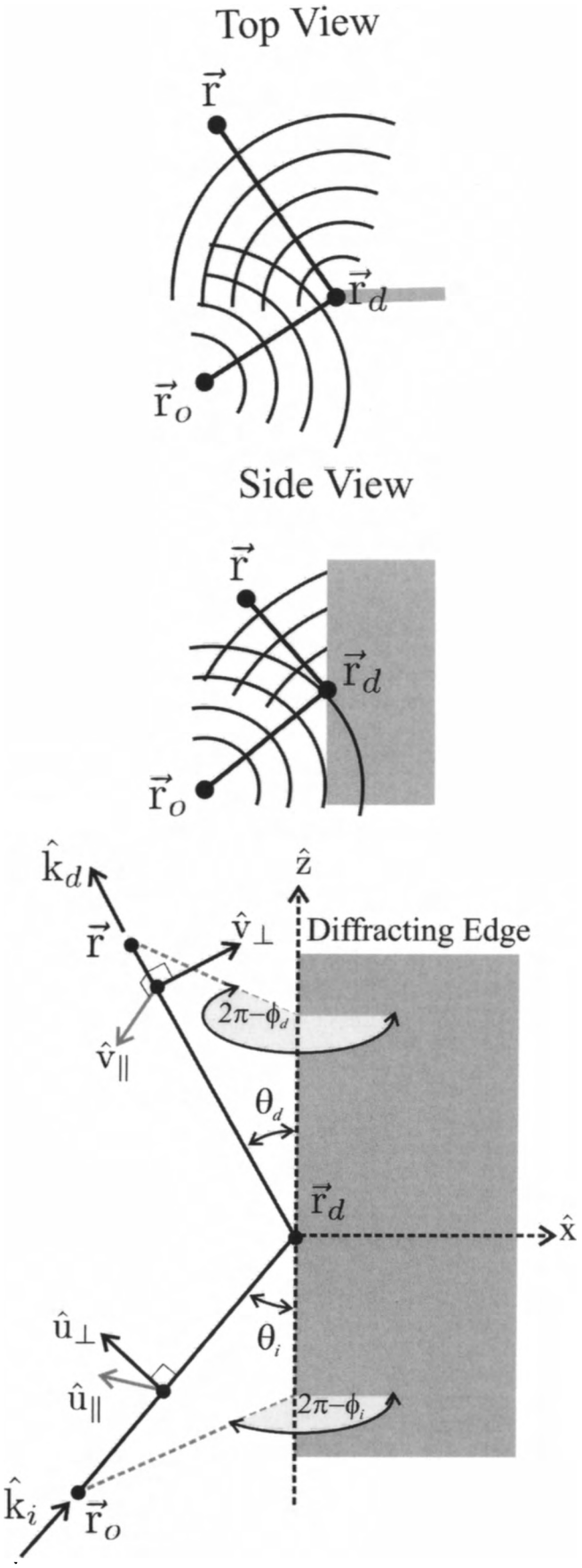

Figure 6. The geometry of the polarization, directions of propagation, and orientation in an oblique edge-diffraction problem. Unit vectors $\hat{\mathrm{k}}_i$, $\hat{\mathrm{u}}_\perp$, and $\hat{\mathrm{z}}$ are co-planar, as are $\hat{\mathrm{k}}_d$, $\hat{\mathrm{v}}_\perp$, and $\hat{\mathrm{z}}$.

To compute the unit-vector decompositions for polarization and direction of travel, refer to Figure 6. This problem is aligned so that the z axis coincides with the diffracting edge. We may thus write unit vectors for the incident direction of propagation, $\hat{\mathrm{k}}_i$, and for the diffracted direction of propagation, $\hat{\mathrm{k}}_d$ as

$$\hat{\mathrm{k}}_i = -\sin\theta_i\cos\phi_i\hat{\mathrm{x}} - \sin\theta_i\sin\phi_i\hat{\mathrm{y}} - \cos\theta_i\hat{\mathrm{z}}, \tag{20}$$

$$\hat{\mathrm{k}}_d = \sin\theta_d\cos\phi_d\hat{\mathrm{x}} + \sin\theta_d\sin\phi_d\hat{\mathrm{y}} + \cos\theta_d\hat{\mathrm{z}}. \tag{21}$$

The unit vectors $\hat{\mathrm{u}}_\perp$ and $\hat{\mathrm{u}}_\parallel$ are defined to be the perpendicular and parallel directions of polarization for the incident wave, and the unit vectors $\hat{\mathrm{v}}_\perp$ and $\hat{\mathrm{v}}_\parallel$ are defined to be the respective directions of polarization for the diffracted wave. With these definitions, we may write the following relationships:

$$\hat{\mathrm{u}}_\parallel = \frac{\hat{\mathrm{z}}\times\hat{\mathrm{k}}_i}{\left\|\hat{\mathrm{z}}\times\hat{\mathrm{k}}_i\right\|},$$

$$\hat{\mathrm{u}}_\perp = \hat{\mathrm{k}}_i\times\hat{\mathrm{u}}_\parallel,$$

$$\hat{\mathrm{v}}_\parallel = \frac{\hat{\mathrm{z}}\times\hat{\mathrm{k}}_d}{\left\|\hat{\mathrm{k}}_d\times\hat{\mathrm{z}}\right\|},$$

$$\hat{\mathrm{v}}_\perp = \hat{\mathrm{k}}_d\times\hat{\mathrm{v}}_\parallel.$$

Though still cumbersome, this geometrical formulation dramatically simplifies the relationship between polarization and diffraction coefficients. This algorithm works well for incident wavefronts that can be described by simple Geometrical Optics expressions. For incident waves with higher-order field structure, it may be necessary to apply *slope* diffraction coefficients for increased accuracy [19].

The geometry of polarization tracking is unnecessary if the scalar KED diffraction coefficient is used. For this case, the dot product of the incident-field vector and the dyadic diffraction coefficient in Equation (19) reduces to a scalar multiplication of field amplitude and KED diffraction coefficient.

3.4 Comparison of the Diffraction Coefficients

In Figure 7, a graph of the GTD diffracted power of both Sommerfeld perpendicular- and parallel-incidence PEC waves is shown, with each normalized against the KED GTD coefficient for the same observation angle. The incidence angle was at $\phi_i = 90°$. Notice that for observations near the shadow boundary, all GTD coefficients are nearly identical, independent of incidence angle. When the observation point drops deeper into the shadow region ($\phi \to 360°$), the parallel-polarization PEC result leads to much more diffracted power than the perpendicular polarization. The converse is true for observations made close to the open aperture in the problem ($\phi \to 180°$).

Perhaps most interestingly, the normally incident KED diffraction coefficient is an *exact* dB average of the two PEC half-plane coefficients across the entire observation area. In the linear scale, the KED diffraction coefficient is then the geometric mean of the two Sommerfeld-based coefficients:

$$\left|D_\Diamond(\phi,\pi/2)\right|^2 = \left|D_\perp(\phi,\pi/2)\right|\left|D_\parallel(\phi,\pi/2)\right|. \tag{22}$$

for all observation angles $180° \le \phi \le 360°$. Despite its approximations, the KED coefficient represents a profoundly useful middle-ground in diffraction problems where polarization or screen composition is unknown. Even more bizarre is that by forcing KED into a geometrical framework, the problematic phase behavior near the plane of the screen is repaired.

Felsen's GTD coefficient $D_\Diamond^{(F)}(\phi,\phi_i)$ for a perfect absorbing half-plane, included in Table 2 and Figure 7 for comparison, also exhibits a blend of behavior for both polarizations of the PEC half-plane – but in an entirely different manner than the KED-based result. Independent of incident angle ϕ_i, the Felsen coefficient resembles the Sommerfeld-perpendicular when $\phi \to 180°$, and resembles the Sommerfeld-parallel when $\phi \to 360°$. Unlike the KED coefficient, the Felsen coefficient does not approach zero on the plane of the screen, thereby violating Kirchhoff boundary conditions. However, the Felsen coefficient does maintain reciprocity by remaining invariant under exchange of the incident angle, ϕ_i, and the observation angle, ϕ; the underlying KED diffracted wave exhibits *non-reciprocal* behavior for certain combinations of incident and observation angles.

4. Example: FM Radio over Terrain

Now let us illustrate how the differences between the diffraction coefficients affect practical radiowave propagation. WREK transmits a 91.1 MHz FM radio signal with an effective isotropic radiated power of EIRP = 54.0 dBW (about 250 kW). To reach one coverage area, the station must rely on double diffraction over the top of two terrain peaks of equal altitude, which can be modeled as 90° wedges, according to the geometry in Figure 8. Calculation of received power using the different diffraction coefficients will illustrate their respective tradeoffs.

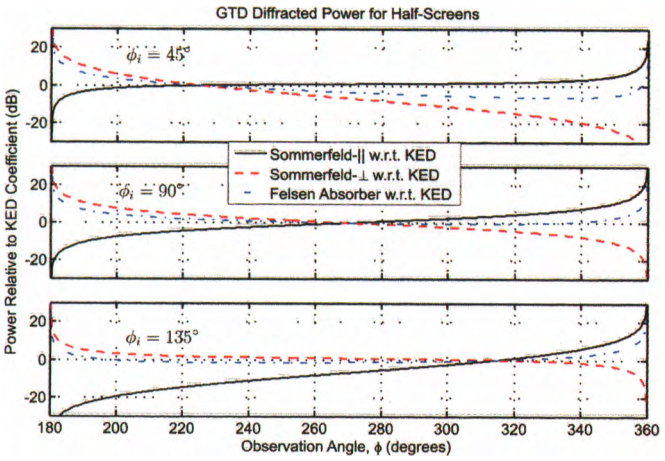

Figure 7. A comparison of GTD coefficients with respect to the KED-based coefficient across observation angles $180° \le \phi \le 360°$. The graphs are for $\phi_i = 45°$, 90° (normal), and 135° incidence.

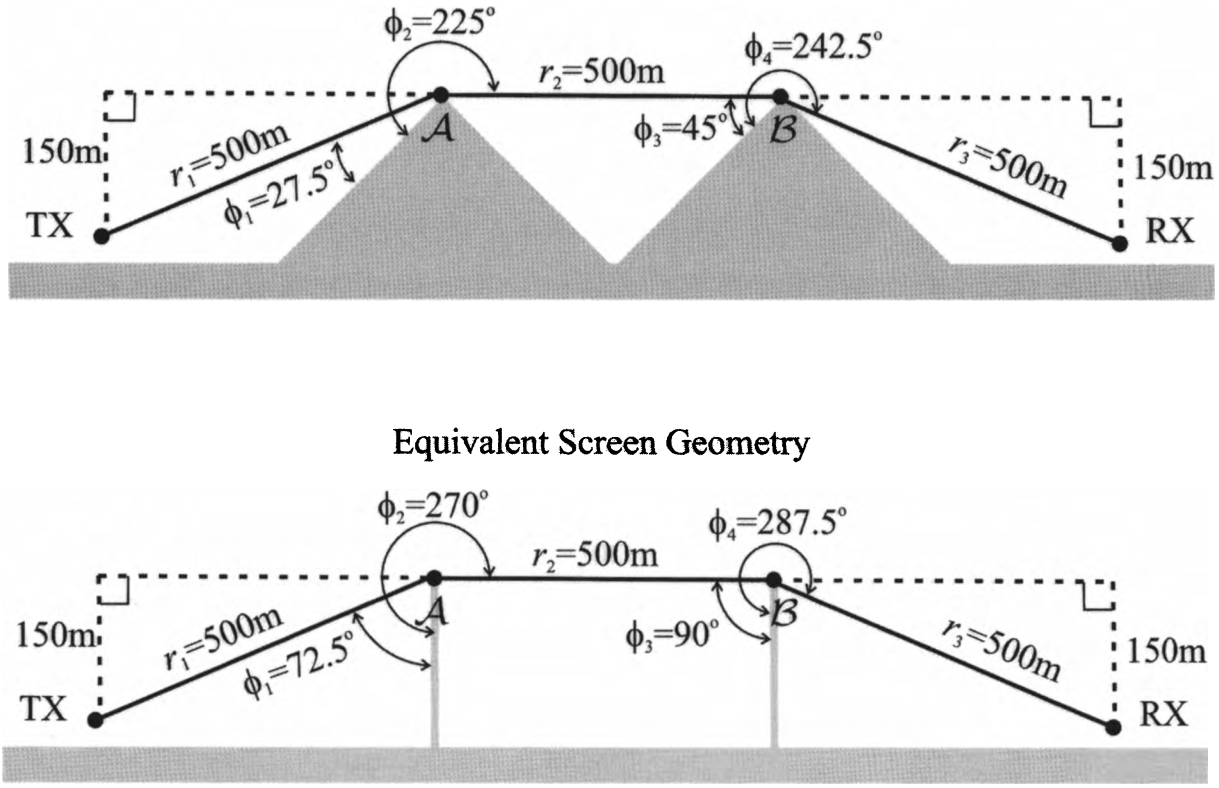

Figure 8. An example of FM radiowave propagation that must diffract over two terrain peaks.

Let us calculate all dimensions, referencing all incident angles to the reflective facets of the two wedges in Figure 8. At point $\mathcal{A}$, the incident wave power is

$$\left(\frac{P_R}{G_R}\right)_{\mathcal{A}} = \text{EIRP}\frac{\lambda^2}{16\pi^2 r_1^2}. \tag{23}$$

When the diffraction coefficient is applied and the first diffracted wave is propagated forward, the wave power at point $\mathcal{B}$ is

$$\left(\frac{P_R}{G_R}\right)_{\mathcal{B}} = \text{EIRP}\frac{\lambda^3 \left|D(\phi_2,\phi_1)\right|^2}{32\pi^3 r_1 r_2 (r_1+r_2)}. \tag{24}$$

Applying the next diffraction coefficient (disregarding any additional reflections and interactions along the way), the second diffracted wave propagates forward to the receiver's location for a received power of

$$\left(\frac{P_R}{G_R}\right)_{\text{RX}} = \text{EIRP}\frac{\lambda^4 \left|D(\phi_2,\phi_1)\right|^2 \left|D(\phi_4,\phi_3)\right|^2}{64\pi^4 r_1 r_2 r_3 (r_1+r_2+r_3)}. \tag{25}$$

The solution in Equation (25) assumes that the second peak lies outside the transition region that surrounds the shadow boundary of the first diffraction peak. Table 3 presents the output of this calculation for a variety of different diffraction coefficients.

Of course, all double-diffraction results in Table 3 yield significantly lower received powers when compared to the −11.9 dBm received in a line-of-sight link of comparable transmitter-receiver separation distance. However, note the difference between the received powers for horizontal ($\perp$) and vertical ($\parallel$) polarizations when the peaks are modeled as diffracting PEC screens: they yield received powers of −85.5 and −80.2 dBm, respectively. The significant difference of 5.3 dB reveals a strong polarization dependence. This difference increases to 12.4 dB when the terrain is modeled as PEC wedges, but the *average* of the two polarization states is almost identical to the average screen-based results.

From these results, we can gather that replacement of wedges with screens in a diffraction problem de-emphasizes polarization dependence, but does not significantly change the average received power [16]. Furthermore, the polarization-averaged received power for the PEC screens of −89.2 dBm is almost identical to the −82.4 dBm of received power predicted by the KED blockage coefficient. The Felsen screen-absorber coefficient also predicts a similar received power of −83.5 dBm.

Table 3. Examples of the received power calculated for the FM-radio double-diffraction example.

Diffraction Treatment	Received Power (dBm)
Line-of-Sight Link	−11.9
PEC Half Plane-$\perp$	−85.5
PEC Half Plane-$\parallel$	−80.2
PEC Wedge-$\perp$	−88.8
PEC Wedge-$\parallel$	−76.4
Felsen Absorber	−83.5
KED Blockage	−82.4

5. Conclusions

Geometrical comparisons of half-screen diffraction problems provide engineers practical insight into the underlying physics and application of diffraction formulas. The GTD or UTD formulations of most screen-diffraction problems are often preferred methods for constructing field solutions, rather than their classical formulations. In fact, this study showed that by forcing KED into a GTD-style framework, some of the skewed behavior is actually *repaired*.

Based on the analysis presented, scalar KED-type diffraction solutions are preferable if the polarization of the radiator is unknown or unpredictable, or if the composition of the diffracting screen is unknown. KED-based GTD provides valuable middle-of-the-road behavior when compared to the range of possible behaviors in other diffraction coefficients. However, if the diffracting edge is truly straight, its composition is highly conductive, and the incident polarization is known, then the Sommerfeld-based GTD or UTD solutions should be applied.

6. Acknowledgements

This study was based on a lecture series in Georgia Tech's ECE 8833: "Advanced Topics in Analytical Electromagnetics" course. Many thanks to class members Kiruthika Deveraj, Chris Edmonds, Josh Griffin, Girish Jain, Lorne Liechty, Ryan Pirkl, and Usman Saed for their participation. Special thanks to Prof. Michael Neve for some extremely helpful ideas, feedback, and encouragement. Part of this content was also prepared (many years ago) as part of a class research project under Prof. Gary S. Brown of Virginia Tech, to whom the author is repeatedly indebted.

7. References

1. M. Born and E. Wolf, *Principles of Optics: Electromagnetic Theory of Propagation, Interference, and Diffraction of Light, Sixth Edition*, New York, Pergamon Press, 1980.

2. C. L. Giovaneli, "An Analysis of Simplified Solutions for Multiple Knife-Edge Diffraction," *IEEE Transactions on Antennas and Propagation*, **AP-32**, 3, March 1984, pp. 297-301.

3. J. Li, J.-F. Wagen, and E. Lachat, "ITU Model for Multi-Knife-Edge Diffraction," *IEE Transactions on Microwaves, Antennas and Propagation*, **143**, 6, December 1996, pp. 539-541.

4. G. Millington, R. Hewitt, and F.S. Immirzi, "Double Knife-Edge Diffraction in Field Strength Prediction," *Inst. of Elec. Eng.*, Monograph 507E, March 1962, pp. 419-429.

5. J. Deygout, "Multiple Knife-Edge Diffraction of Microwaves," *IEEE Transactions on Antennas and Propagation*, **AP-14**, 4, July 1966, pp. 480-489.

6. J. Deygout, "Correction Factor for Multiple Knife-Edge Diffraction," *IEEE Transactions on Antennas and Propagation*, **AP-39**, 8, August 1991, pp. 1256-1258.

7. H. Mokhtari, "Comprehensive Double Knife-Edge Diffraction Computation Based on the Complete Fresnel Theory and a Recursive Series Expansion Method," *IEEE Transactions on Vehicular Technology*, **48**, 2, March 1999, pp. 589-592.

8. B. A. Davis and G. S. Brown, "Diffraction of a Randomly Rough Knife Edge," *IEEE Transactions on Antennas and Propagation*, **AP-50**, 12, December 2002, pp. 1769-1778.

9. G. D. Durgin, "Practical Geometrical Behavior of Knife-Edge Diffraction," IEEE International Symposium on Antennas and Propagation, San Diego CA, July 2008.

10. R. J. Luebbers, "Finite Conductivity Uniform GTD Versus Knife Edge Diffraction in Prediction of Propagation Loss," *IEEE Transactions on Antennas and Propagation*, **AP-32**, 1, pp. 70-76, January 1984, pp. 70-76.

11. W. Honcharenko and H. L. Bertoni, "Prediction of RF Propagation Characteristics in Buildings Using 2D-Ray Tracing," IEEE 45th Vehicular Technology Conference, Chicago IL, July 1995, pp. 429-433.

12. M. J. Neve and G. B. Rowe, "Mobile Radio Propagation Prediction in Irregular Cellular Topographies Using Ray Methods," *IEE Proceedings on Microwaves, Antennas, and Propagation*, **142**, 6, December 1995, pp. 447-451.

13. J. B. Keller, "Geometrical Theory of Diffraction," *Journal of the Optical Society of America*, **52**, 2, February 1962, pp. 116-130.

14. G. L. James, "An Approximation to the Fresnel Integral," *Proceedings of the IEEE*, **67**, 4, April 1979, pp. 677-678.

15. R. G. Kouyoumjian and P. H. Pathak, "A Uniform Geometrical Theory of Diffraction for an Edge in a Perfectly Conducting Surface," *Proceedings of the IEEE*, **62**, 11, November 1974, pp. 1448-1461.

16. H. L. Bertoni, *Radio Propagation for Modern Wireless Systems*, Upper Saddle River, NJ, Prentice Hall, 2000.

17. L. B. Felsen and N. Marcuvitz, *Radiation and Scattering of Waves*, Upper Saddle River, NJ, Prentice Hall, 1973.

18. C. A. Balanis, *Advanced Engineering Electromagnetics*, New York, John Wiley & Sons, 1989.

19. R. G. Kouyoumjian, "The Geometrical Theory of Diffraction and Its Applications," in R. Mittra (ed.), *Numerical and Asymptotic Techniques in Electromagnetics*, New York, Springer, 1975.